Green synthesis of TiO_2 nanoparticles for furfural production by photohydrolysis of unexplored residual biomass: the nejayote

Janneth López-Mercado (jannlopezm@gmail.com)
Universidad de La Ciénega del Estado de Michoacán de Ocampo
Martha-Isabel González-Domínguez
Universidad de La Ciénega del Estado de Michoacán de Ocampo
Francisco-Javier Reynoso-Marin
Universidad de La Ciénega del Estado de Michoacán de Ocampo
Brenda Acosta
Cátedras CONACYT, Universidad Autónoma de San Luis Potosí
Elena Smolentseva
Universidad Nacional Autónoma de México
Apolo Nambo
University of Louisville

Article

Keywords: TiO2 nanoparticles, green synthesis, photohydrolysis, nejayote, furfural

Posted Date: April 18th, 2023

DOI: https://doi.org/10.21203/rs.3.rs-2739045/v1

Version of Record: A version of this preprint was published at Scientific Reports on September 16th, 2023.
See the published version at https://doi.org/10.1038/s41598-023-41529-z.

Abstract

Green synthesis is characterized by using plants' secondary metabolites (S-Met) to reduce metal ions into metallic atoms, which are subsequently nucleated and agglomerated, forming the nanoparticles (NPs). Thereby, the significant diminishing in producing toxic waste during the green synthesis approach may be considered an environmentally friendly alternative. In the present work, titania (TiO_2) NPs were greenly synthesized using *Ricinus Communis* (RC), *Moringa Oleifera* (MO) or *Bougainvillea Spectabilis* (BS) plant extracts. Obtained nanoparticles were characterized using XRD, SEM, EDS, BET, XPS and UV-vis techniques. The physicochemical and electronic properties of synthesized nanoparticles were improved concerning the reference material. The surface area increased up to 17 times, accompanied by a decrease in crystal size (~50%) and gap energy value. Furthermore, the photocatalytic performance of the obtained samples was evaluated in the furfural production from nejayote, an unexplored industrial residual biomass. The furfural yield was twice higher using the sample obtained from the BS metabolites than those obtained with the other S-Met, attributed to the preferable formation of xylose over other pentoses. This work proved the viability of nanomaterial synthesis using common plants abundant in Latin-American applied for the waste transformation coming from an overall process such as nixtamalization, the nejayote.

1. Introduction

The application of TiO_2 NPs for several photocatalytic processes is widely used for the degradation of organic and inorganic compounds, such as lignin (paper industry) [1, 2], orange II dye (textile industry) [3], Cr^{+6} (leather manufacturing) [4], rhodamine B (chemical industry) [5] presented in wastewater. The photocatalytic efficiency for the degradation of the compounds mentioned above was directly correlated to the optoelectronic and physicochemical properties of TiO_2 obtained during the nanomaterial synthesis. [6]

TiO_2 NPs are synthesized through various methodologies. [7–9] Among the most recognized are sol-gel [2, 10], hydrothermal [11, 12], combustion [13], vapor phase [14, 15], controlled precipitation, polymer precursor [16], etc. However, the application of such methodologies requires the use of solvents, reducing agents and stabilizing materials, which can generate various toxic or harmful compounds; moreover, it increases the costs of production of TiO_2 NPs. Green synthesis may be considered as an alternative way to reduce health risks and environmental impact during the synthesis of nanomaterials. [17] This methodology allows exploring the potential of certain plant extracts known as S-Met (terpenes, essential oils, flavonoids, phenols, etc.) to reduce metal ions and generate stable nanoparticles with unique morphologies. [4] Until now, green synthesis has been mainly applied to produce noble metals (Ag, Au, Pt and Pd, Cu) and metal oxides (Zn and Ti) NPs [18, 19]. The source of S-Met can be associated with the demand for specific compounds (polyphenols, flavonoids, acids, etc.) required for the synthesis of NPs and their final application, as well as the geographical conditions and variety of available plants. For example, plants of historical relevance for disease treatment (Indian rosewood and gooseberry, tea

leaves, etc.) are widely studied for the synthesis of metal NPs with antimicrobial applications. [19] Some researchers reported the use of S-Met, extracted from BS, MO and RC, for the synthesis of silver NPs with various applications. [20, 21] Nowadays, the green synthesis of TiO_2 NPs using those extracts has to be extensively studied.

The anatase phase of crystalline TiO_2 presents photocatalytic properties under UV radiation. It is extensively employed in environmental remediation, clean energy generation, organic synthesis, etc. [5, 22] Other areas of opportunity for applying such versatile materials may be converting lignocellulose matter to high-value-added chemicals, such as furan compounds. [23] Furan compounds are considered platform molecules because of their broad range of applications. Furfural is one of the most studied furan compounds, which may be obtained through the acid hydrolysis of 5-carbon sugars derived from hemicellulose and pectin polysaccharides. [24, 25] These 5-carbon sugars are found in various biomasses and/or food processing wastes. A typical food processing technique is corn nixtamalization for tortilla production in México and some other countries of Central America, the United States of America, Asia and Europe. [26] Nejayote is a waste stream of alkaline water produced during the industrial nixtamalization process, which is considered hazardous. Currently, there is no process for nejayote treatment to reduce its dangerousness. This waste stream with high pH is also loaded with organic corn compounds that can be used as precursors for producing furan compounds such as furfural or 5-hydroxymethyl furfural. Typically, such reactions are performed in an aqueous phase and require the addition of water to transform sugars into furans. Note that both substrates are present in the nejayote.

The present work compares the use of different S-Met plant extracts obtained from RC, MO and BS plants of the marshland region of Chapala, México, in the green synthesis of TiO_2 NPs. Physicochemical and electronic properties of greenly synthesized TiO_2 NPs are discussed, as well as their potential use for furfural production by photohydrolysis of the unexplored nejayote, a typical industrial residual biomass in Latin America. Commercial TiO_2 (comm TiO_2) was also analyzed parallelly and presented as reference material.

2. Materials And Methods

2.1 Materials

Sulfuric acid (H_2SO_4 Sigma Aldrich), sodium bicarbonate ($NaHCO_3$, Sigma Aldrich) hydrochloric acid (HCl Sigma Aldrich), magnesium (Mg, Golden Bell), titanium isopropoxide ($Ti[OCH(CH_3)_2]_4$, Sigma Aldrich) and comm TiO_2 (TiO_2, Fermont) were used as reagents for the analysis of S-Met and TiO_2 NPs synthesis. The furfural (C H OCHO, Sigma Aldrich) was used as the standard for the calibration curve. The RM, MO and BS plants were collected nearest Chapala Lake, in Jalisco, México. For the photohydrolysis reaction, the nejayote sample wasobtained from a local industry in Sahuayo, Michoacán, México. Nejayote is considered fresh and useful up to three days before its collection.

2.2 Metabolites extraction

Different sections of each plant were used for the S-Met extraction, flowers and bracts from BS, and leaves from RC and MO. The methodology commonly applied to extract the S-Met is reported.[20] In the present work, the extraction conditions were modified to increase the efficiency of the process. Briefly, each plant extract was obtained by mixing 20 g of the plant with 100 mL of water. Then, the mixture was heated up to 90°C and kept for 10 min. Finally, the aqueous extract was separated by vacuum filtration and kept refrigerated until use. [27] All methods were performed in accordance with the relevant guidelines and regulations.

2.3 Qualitative phytochemical analysis of extracts

Each plant extract underwent a phytochemical screening to know the phytoconstituents of the obtained S-Met. The presence of flavonoids, tannins, phenols, quinones and saponins was evaluated following well-known methodologies such as Shinoda, Foam tests, $FeCl_3$ test and others, described. [28–30]

2.4 Nanoparticles green synthesis

Titanium isopropoxide (12 mL) was mixed with 78 mL of distilled water and 10 mL of the S-Met plant extract obtained from each selected plant. The formed suspension was kept at 50°C for 4 h under magnetic stirring. Subsequently, the obtained product was washed with distilled water and dried at 60°C overnight. Finally, the samples were calcined at 500°C for 3 h. The powdered sample was collected and saved for later testing and characterization.

2.4 Physicochemical characterization

The morphology and elemental composition of the greenly synthesized TiO_2 NPs were studied by scanning electron micrographs and X-Ray energy dispersion spectra, respectively, obtained with a JSM-6610-LV microscope, JEOL. Structural analysis of samples was performed using X-ray diffraction patterns collected in a D8 Avance A25 Bruker X-Ray diffractometer equipped with CuKα radiation. Textural properties of titania samples were determined by the N_2 thermal adsorption measurements using TriStar II-3020 equipment, Micromeritics. Before the analysis, the samples were dried under vacuum (10^{-3} torr) at 300°C for 3h using a VacPrep 061-Sample degas system, Micromeritics. Obtained isotherms were analyzed via the Brunauer-Emmet-Teller (BET) and Barrett-Joyner-Halenda (BJH) models for the surface area and porosity determination, respectively. The optical characterization of the powder samples was determined by UV-vis spectroscopy in diffuse reflectance mode using an UV-3600 Plus UV-VIS-NIR spectrophotometer, Shimadzu, equipped with an integrating sphere. The samples were placed in a quartz cell with 2 mm in the light path for the measurement. The electronic state of prepared samples was studied by the XPS technique with a PHOIBOS spectrometer, SPECS, with 150 WAL hemispherical energy analyzer and a monochromatic source (AlKα Xray, 1486.6 eV).

2.5 Photocatalytic evaluation

2.5.1 Nejayote characterization

Fresh nejayote (100 mL) was treated with 4%w of H_2SO_4 at 200°C for 2 h, using an autoclave. Then, the obtained solution/suspension was analyzed by means of liquid chromatography using an Ultimate 300 High-Pressure Liquid Chromatographer, Thermo Scientific, equipment to determine the presence of sugars. Additionally, 100 mL of fresh nejayote were diluted in 100 mL of water and then centrifuged. The supernatant was separated while the precipitated solids were calcined at 500°C for 5 h. Calcined samples were analyzed by EDS to determine the inorganic matter.

2.5.2 Nejayote photohydrolysis

The photocatalytic performance of the obtained TiO_2 NPs was evaluated at the photohydrolysis of nejayote to produce furfural. Reactions were carried out in a cylindrical quartz batch reactor (1 L) under controlled stirring (400 rpm) at room temperature. Typically, 1g of the sample was dispersed in 800 mL of nejayote. Before the light irradiation, the reaction mixture was stirred for 30 min to reach the adsorption equilibrium. Then, the UV-light lamp (365 nm) was turned on. The reaction progress was monitored by analyzing the products at different times (5, 15, 30, 45, 60 and 90 minutes). The furfural concentration each time was determined using a Perkin Elmer Clarus 680 model gas chromatograph coupled to a mass spectrometer (GC-MS).

3. Results And Discussion

3.1 Metabolites characterization

It is well-known that S-Met assists the biosynthesis of metal NPs acting as a reducing and/or stabilizing agents. [31] The qualitative information on phytochemical constituents of obtained S-Met used in the green synthesis of TiO_2 NPs is shown in Table 1. The presence of flavonoids, saponins, tannins and phenols characterized the S-Met extracts from the three plants. The absence of essential oils and fatty substances was observed for all analyzed plants; meanwhile, flavones were only found in RS and MO extracts. The slight variations in the constituents found for each plant may be attributed to using different plant parts for the extraction, such as leaves from RC and MO, while flowers and branches for BS. [31] Flavonoids and phenols are considered potential reducers of metallic precursors. [32] Indeed, Bharathi [20] showed that flavonoids and phenols obtained from BS are the principal for forming silver nanoparticles by reducing silver nitrate. On the other hand, Mintiwab and Jeyaramraja reported that flavonoids, tannins, saponins, alkaloids, triterpenes and steroids extracted from RC leaves allow the reduction and stabilization of silver nanoparticles. [32] Moodley reported that flavones, terpenoids and polysaccharides obtained from MO leaves are primarily responsible for the reduction and stabilization of silver [21] and TiO_2 NPs [33]. It is expected that found constituents (flavonoids, saponins, tannins and phenols) can reduce the titanium precursor salt to titanium ion intermediates for their further conversion into TiO_2 NPs.

Table 1
Qualitative information on phytochemical constituents of secondary metabolites.

Method	Phytochemical constituent	*Bougainvillea spectabilis*	*Moringa oleífera*	*Ricinus communis*
Shinoda test	Flavonoids	+	+	+
Shinoda test with heat	Flavonoids	+	+	+
H_2SO_4 test	Flavone	-	+	+
	Quinones	+	-	-
Foam test (5 minutes)	Saponins	+	+	+
Foam test (30 minutes)	Saponins	+	+	+
$NaHCO_3$ test	Saponins	+	+	+
HCl test	Tannins and phenols	+	+	+
$FeCl_3$ test	Tannins and phenols	+	+	+
Essential oils and fatty substances	Essential oils and fatty substances	-	-	-

* -Absent, + Present

3.2 Nanoparticles characterization

The elemental analysis of TiO_2 samples confirmed the presence of titanium and oxygen mostly (Table S1). However, some traces of potassium were found in the samples obtained with S-Met plants extract. The latter may be assigned to the chemical composition of plants, where inorganic matter, such as potassium, indicates that the extracellular inorganic moieties are absorbed in the TiO_2 NPs surface. [33, 34] Nevertheless, its contribution was insignificant to interfere with the sample properties, such as the morphology or composition.

Figure S1 presents the typical SEM micrographs of the TiO_2 NPs samples prepared from different plant extracts and comm TiO_2 as reference. The green synthesis approach resulted in a quasispherical shape of TiO_2 NPs with a size below 100 nm. In comparison, comm TiO_2 was characterized with larger aggregates (up to 300 nm) (Figure S1). According to the micrographs analysis, the diameter of the formed TiO_2 NPs was 30, 40 and 25 nm when BS, MO and RC were used, respectively. Despite the slight differences in the qualitative characterization of the S-Met extract (see Table 1), it seems that both the S-Met dispersion and solubility in the reaction media are responsible for the morphology inhomogeneity for the obtained TiO_2 NPs, as was discussed for the Ag nanoparticles synthesis from BS and MO extracts. [20, 21] Indeed, some studies related to the green synthesis of TiO_2 NPs, using the same Ti precursor

($Ti[OCH(CH_3)_2]_4$), resulted in the formation of heterogeneous morphology accompanied by the contribution of NPs with different sizes (even up to micrometers) [35], unless a tensoactive is used.[36]

Figure 1 shows the X-ray diffraction patterns for the greenly synthesized samples compared to that for the reference comm TiO_2 powder. All samples were characterized with well-distinguishable reflections between 20°-90° of 2θ. However, the reflections for TiO_2 prepared by green synthesis were less intensive and broader than that for commercial sample. XRD analysis revealed the preferential formation of the TiO_2 anatase phase. The most intensive peaks were located at 25° and 48° of 2θ, corresponding to [101] and [200] crystallographic planes of the TiO_2 anatase phase, according to the PDF 00-064-0863 card. The low intensity and high broadness of the peaks for nanostructured TiO_2 may be attributed to the presence of TiO_2 crystals with the nanodomain size, which formation was promoted by the active species from the metabolites used, as reported by Logeswari et al., during the green syntheses of silver nanoparticles from organic aqueous extracts of different plants as well as *Solanum tricobatum, Syzygium cumini, Centella asiatica* and *Citrus sinensis.*[37]The crystal formation processes are based on the titania primary species nucleation principles, so their ordered growth in one direction is limited by the components presented in the metabolites. The crystal size of TiO_2 was estimated by Scherrer´s equation (see Table 2). The results confirmed that all greenly synthesized TiO_2 NPs were composed of relatively small crystals around 20 nm, while the reference TiO_2 sample was characterized with a bigger crystal size (41 nm). These results correlate well with the SEM data.

Table 2
Summary of physicochemical properties of TiO_2 nanoparticles prepared via green synthesis using different plant extracts.

TiO_2 source	Crystallite size*, nm	Gap energy values**, eV	Specific surface area, m^2/g	Pore volume, cm^3/g
Bougainvillea spectabilis	20	3.20	113	0.21
Moringa oleífera	25	3.22	124	0.21
Ricinus communis	18	3.25	115	0.19
Commercial	41	3.29	7	0.007
* Calculated using the Scherrer´s equation on the peak at 2θ = 25.				
** Estimated by the Tauc plot method.				

Figure 2 presents the adsorption-desorption isotherms for all samples. The isotherms for the greenly synthesized samples were characterized by a Type 4. At the same time, the comm TiO_2 obtained isotherm was a Type III, commonly assigned to mesoporous and nonporous materials, according to the IUPAC classification. In addition, the hysteresis loop shape (H1) revealed the presence of cylindrical-like pore channels. [30] Therefore, thermal physisorption of N_2 for prepared TiO_2 NPs presented significant

differences in the amount of gas adsorbed in comparison with the reference commercial sample (see Fig. 2). The latter coincided well with the remarkable improvement of the specific surface area values for green synthesized TiO_2 NPs (see Table 2). The TiO_2 NPs prepared by green synthesis were characterized with similar values of surface area (~ 120 m^2/g) and pore volume (~0.21 m^3/g); meanwhile, for the comm TiO_2 sample, these values were lower (7 m^2/g and 0.007 m^3/g, respectively). Furthermore, applying the BJH model for the physisorption data displayed an average porous size of around 5.5 nm for all synthesized samples (Table 2). Note that the TiO_2 samples prepared using RC and MO demonstrated two types of pores (4.2 and 6.3 nm, respectively). Thus, the applied green synthesis allowed the formation of relatively small TiO_2 nanocrystals to form TiO_2 NPs in the anatase phase with a remarkable enhancement of the surface area. Furthermore, the mesoporous nature of the greenly synthesized TiO_2 NPs was revealed. Therefore, it may conclude that the green synthesis affects the textural properties of the prepared TiO_2 NPs, which makes them functional for the proposed photocatalytic reaction because no mass transport limitations are expectable.

The high-resolution XP spectra of comm TiO_2 (D) and prepared samples BC (A), MO(B) and RC (C)for the Ti2p region are presented in Fig. 3. The TiO_2 sample, the Ti2p spectrum is characterized by two spin-orbit components, $Ti2p_{3/2}$ and $Ti2p_{1/2}$, separated by 5.7 eV [38] exhibited several doublets attributed to different Ti oxidation states such as Ti^{3+} or Ti^{4+} .[39]For all samples, the obtained Ti2p core level spectra presented two symmetric bands centered at binding energies of c.a. 458.5 and 464 eV assigned to $Ti2p_{3/2}$ and $Ti2p_{1/2}$, respectively, for the Ti^{4+} chemical state. Similar results are cited in the literature for TiO_2 prepared via green methods [39, 40, 41] Furthermore, a Ti^{3+} oxidation state is reported when surface defects are formed [39] or dopants are incorporated into the TiO_2 green synthesis procedure. In contrast, the Ti^{4+} oxidation state is found when only plant extracts are used. [42, 43] Thus, it was confirmed that the maximum oxidation state of Ti for the greenly synthesized TiO_2 NPs was reached. However, the plant extract did not affect the Ti chemical state achieved under green synthesis.

The UV-vis absorption spectra of the synthesized samples were similar to the comm TiO_2 (see Fig. 4-A), characterized by an absorption edge in the near UV region due to the charge transfer between Ti and O. It is well-known that the band gap energy values are associated with the photocatalytic performance of titanium. The band gap energy for these materials was estimated from the UV-vis absorption edge wavelength of the interband transition according to the Tauc plot method described in [44] (see Fig. 4-B). The band gap energy value for comm TiO_2 was 3.29 eV, which is in good agreement with the literature data for the TiO_2 oxide in the anatase phase (~ 3.30 eV).[45] Meanwhile, the values obtained for the greenly synthesized TiO_2 samples were 3.20, 3.22 and 3.25 eV for the samples obtained from BS, MO and RC, respectively (see Table 2). Those results agree with those reported for TiO_2 NPs prepared via a green approach.[4] The decreased optical band gap for greenly synthesized TiO_2 NPs makes it possible to propose that e- and h + pairs can be generated, promoting photocatalysis. Usually, synthesized TiO_2 NPs are characterized by a decrease in band gap energy value because the structure formation is hardly

influenced by the ordered aggregation of fine crystals, as was previously discussed. Instead, these fine crystals promoted the presence of surface defects that decreased the band gap energy value.[44] Therefore, the estimated band gap energy values were influenced by forming domains with several sizes promoted by the phytochemical components presented in the extract plant. The latter was previously confirmed by the crystal size calculations (see Table 2).

3.3 Photocatalytic evaluation

3.3.1 Nejayote characterization

The composition analysis of nejayote revealed 32.5% of pentoses (ribose, arabinose, and xylose) and 47% of hexoses (glucose). Another 20.5% was attributed to other compounds such as lignin, inorganic matter (Ca, mainly), proteins, etc.

Table 3 shows the determination of elements in the solid sample of nejayote and ash (product of heat treatment of the nejayote solid sample). The results showed the high contribution of calcium and oxygen, characteristic of ¨calcium oxide¨, which is used for the ¨nixtamalization¨ process and the generation of nejayote (wastewater). In addition, it was observed that there was no carbon in the ash sample, which proves the absence of organic matter (polysaccharides and/or sugars).

Table 3
Elemental evaluation of organic and inorganic matter in the nejayote.

Sample	%C	%Ca	%Cl	%K	%O
Nejayote (solids)	36.61	48.95	0.46	1.46	12.54
Nejayote (ash)		35.24	1.21	7.93	53.44

3.3.2 Furfural production

Figure 5 displays the furfural yields obtained from the nejayote photohydrolysis using the greenly synthesized TiO_2 NPs and comm TiO_2 as catalysts. All samples were characterized by a furfural production during the first 30 min. The order of the activity of the samples was BS>MO≈comm TiO_2>RC. TiO_2 NPs obtained using S-Met from BS displayed a 45% furfural yield. The feedstock employed, the nejayote, instead of high-purity xylose, made this result unprecedented. Indeed, the furfural yield reached by the BS sample was 0.6 and 0.5 times compared to those presented by Alonso et al. [46] and Gallo et al. [47], respectively, when xylose was used. Additionally, the reaction conditions in the present work were environmentally beneficial because 1) no extra water or energy to raise the temperature of the reactor was required [46, 47]; and 2) no additional solvents such as GVL, toluene, THF, etc. [46–48] were used.

The furfural production was very low for the RC sample, with a yield below 6% during the reaction. On the contrary, the MO and comm TiO_2 samples demonstrated similar behavior for the furfural production with relatively constant product formation (~ 25%). The BS sample revealed unstable behavior in the curse of

the reaction. The low output of the furfural for the RC sample may be attributed to differences in the polysaccharides rupture (glycosidic bond) pathways, which can produce a different ratio of xylose, arabinose, and ribose. [48] The latter may impact the product distribution in their subsequent hydrolysis. Furfural production is favored at high ratios of xylose, which has been described as a molecule with an isomerization process that leads to faster Furfural production through xylulose and lyxose,[[48] Additionally, nejayote contains relatively big molecules, such as polymers and proteins, that can affect the depolymerization and dehydration processes involved in furfural synthesis. From this perspective, the pore size and morphology of greenly synthesized TiO_2 NPs may affect the diffusion of the molecules due to the nature of the feedstock.

Note that the performance of the MO sample is comparable with that presented for the comm TiO_2. The comm TiO_2, characterized by low surface area, mainly contributes to the external surface area. The latter may explain the lack of diffusional limitations of byproducts or impurities. In contrast, all greenly synthetized TiO_2 NPs displayed a smaller particle size and higher surface area that promote the diffusion of the reactive. However, the MO samples present the largest crystal size compared to the green synthesized BS and RC. The big crystal size accompanied by the small particle size could promote the formation of external active sites, favoring the photocatalytic activity of the material particles' external surface, leading to a similar behavior to that of the comm TiO_2.

4. Conclusions

The effect of the plants' S-Met on the physicochemical properties and photocatalytic performance of the greenly synthesized TiO_2 NPs is shown. The S-Met extract from the BS plant to synthesize TiO_2 NPs is used for the first time, but this is different for RC and MO metabolites. The crystal size and gap energy values decreased; meanwhile, the surface area increased up to 17 times in the greenly synthesized TiO_2 NPs concerning the comm TiO_2. For the first time, the furfural production is investigated via the photohydrolisis of the nejayote, unexplored residual biomass, applying greenly synthesized TiO_2 NPs. The maximum furfural yield achieves 45% on the BS catalysts. The furfural yield reached by the greenly synthesized TiO_2 NPs is comparable and 2 times superior to the reference comm TiO_2, following the BS>MO≈comm TiO_2>RC trend. The intrinsic nejayote composition and the catalysts surface both interfere with the polysaccharide fragmentation through the glucoside bond breakage to form pentoses and their subsequent transformation into furfural. The nejayote photohydrolisis reaction on the greenly synthesized TiO_2 NPs presents a comparable furfural yield to those reported when a high-purity xylose reagent is used.

The Chapala, México marshland region provides beneficial S-Met extracts to promote the synthesis of active, sustainable and environmentally friendly catalysts. Furthermore, this work shows the potential to exploit a complex feedstock, promoting the lignocellulosic residual biomass valorization, to produce highly valuable compounds, such as furfural.

Declarations

Acknowledgments

Authors acknowledge the technical support from Victor Garcia, the Energy Engineering students William Jesús Hernández Valdovinos and Elizabeth Gil Manzo, the Nanotechnology Engineering students Juan Manuel Calderón Sánchez and Rogelio Barocio Salcido of Universidad de La Ciénega del Estado de Michoacán de Ocampo. This work was funded by Universidad de La Ciénega del Estado de Michoacán de Ocampo ¨UCEMICH¨ (Research projects, call 2020) and CONACYT through the projects A1-S-45958, 302286 and 299812, Mantenimiento de Infraestructura Científica en Laboratorios Nacionales 2020-314931, 2021-315911, FAI-UASLP, COPOCYT (escrow 23871) and SENER-CONACYT (117373). The authors thank the access and use of the equipment in the Laboratorio Nacional de Análisis Físicos, Químicos y Biológicos-CIACYT, UASLP. Brenda Acosta sincerely acknowledges the Investigadoras e Investigadores por México, CONACYT program.

Data Availability

The datasets generated and/or analysed during the current study are not publicly available due, but could be available from the corresponding author on reasonable request.

References

1. Ahmad, W., Singh, A., Jaiswal, K. K., & Gupta, P. (2021). Green synthesis of photocatalytic TiO_2 nanoparticles for potential application in photochemical degradation of ornidazole. *Journal of Inorganic and Organometallic Polymers and Materials*, 31(2), 614-623. doi.org/10.1007/s10904-020-01703-6.
2. Rangel, R., Mercado, G. J., Bartolo-Pérez, P., & García, R. (2012). Nanostructured-[CeO_2, La_2O_3, C]/TiO_2 catalysts for lignin photodegradation. *Science of Advanced Materials*, 4(5-6), 573-578. doi.org/10.1166/sam.2012.1321
3. Bhattacharyya, A., Kawi, S., & Ray, M. B. (2004). Photocatalytic degradation of orange II by TiO_2 catalysts supported on adsorbents. *Catalysis Today*, 98(3), 431-439. doi.org/10.1016/j.cattod.2004.08.010.
4. Goutam, S. P., Saxena, G., Singh, V., Yadav, A. K., Bharagava, R. N., & Thapa, K. B. (2018). Green synthesis of TiO_2 nanoparticles using leaf extract of Jatropha curcas L. for photocatalytic degradation of tannery wastewater. *Chemical Engineering Journal*, 336, 386-396. doi.org/10.1016/j.cej.2017.12.029.
5. Voisin, H., Falourd, X., Rivard, C., & Capron, I. (2021). Versatile nanocellulose-anatase TiO_2 hybrid nanoparticles in Pickering emulsions for the photocatalytic degradation of organic and aqueous dyes. *JCIS Open*, 3, 100014. doi.org/10.1016/j.jciso.2021.100014.

6. Viana, M. M., Soares, V. F., & Mohallem, N. D. S. (2010). Synthesis and characterization of TiO_2 nanoparticles. *Ceramics International*, 36(7), 2047-2053. doi.org/10.1016/j.ceramint.2010.04.006.
7. Malekshahi Byranvand, M., Nemati Kharat, A., Fatholahi, L., & Malekshahi Beiranvand, Z. (2013). A review on synthesis of nano-TiO_2 via different methods. *Journal of nanostructures*, 3(1), 1-9.
8. Gupta, S., & Tripathi, M. (2012). A review on the synthesis of TiO_2 nanoparticles by solution route. *Open Chemistry*, 10(2), 279-294. doi.org/10.2478/s11532-011-0155-y.
9. Nyamukamba, P., Okoh, O., Mungondori, H., Taziwa, R., & Zinya, S. (2018). Synthetic methods for titanium dioxide nanoparticles: a review. titanium dioxide-material for a sustainable environment, 151-1755. dx.doi.org/10.5772/intechopen.75425.
10. Pecchi, G., Reyes, P., Sanhueza, P., & Villasenor, J. (2001). Photocatalytic degradation of pentachlorophenol on TiO2 sol–gel catalysts. *Chemosphere*, 43(2), 141-146. doi.org/10.1016/S0045-6535(00)00265-4.
11. Chen, M., Ma, C. Y., Mahmud, T., Lin, T., & Wang, X. Z. (2012). Population balance modelling and experimental validation for synthesis of TiO_2 nanoparticles using continuous hydrothermal process. *In Advanced Materials Research* (Vol. 508, pp. 175-179). Trans Tech Publications Ltd. doi.org/10.4028/www.scientific.net/AMR.508.175.
12. Ahn, K. H., Lee, Y. H., Kim, M., Lee, H. S., Youn, Y. S., Kim, J., & Lee, Y. W. (2013). Effects of surface area of titanium dioxide precursors on the hydrothermal synthesis of barium titanate by dissolution–precipitation. *Industrial & Engineering Chemistry Research*, 52(37), 13370-13376. doi.org/10.1021/ie401161x.
13. Wu, J., Li, C., Zhao, X., Wu, Q., Qi, X., Chen, X., ... & Cao, Y. (2015). Photocatalytic oxidation of gas-phase Hg0 by CuO/TiO_2. *Applied Catalysis B: Environmental*, 176, 559-569. doi.org/10.1016/j.apcatb.2015.04.044.
14. Avril, L., Bourgeois, S., de Lucas, M. M., Domenichini, B., Simon, P., Addou, F., ... & Imhoff, L. (2015). Thermal stability of Au–TiO2 nanocomposite films prepared by direct liquid injection CVD. *Vacuum*, 122, 314-320. doi.org/10.1016/j.vacuum.2015.06.018.
15. Lee, H., Song, M. Y., Jurng, J., & Park, Y. K. (2011). The synthesis and coating process of TiO2 nanoparticles using CVD process. *Powder technology*, 214(1), 64-68. doi.org/10.1016/j.powtec.2011.07.036.
16. Malagutti, A. R., Mourao, H. A., Garbin, J. R., & Ribeiro, C. (2009). Deposition of TiO_2 and Ag: TiO_2 thin films by the polymeric precursor method and their application in the photodegradation of textile dyes. *Applied Catalysis B: Environmental*, 90(1-2), 205-212. doi.org/10.1016/j.apcatb.2009.03.014.
17. Zamri, M. S. F. A., & Sapawe, N. (2019). Kinetic study on photocatalytic degradation of phenol using green electrosynthesized TiO2 nanoparticles. *Materials Today: Proceedings*, 19, 1261-1266. doi.org/10.1016/j.matpr.2019.11.131.
18. Jadoun, S., Arif, R., Jangid, N. K., & Meena, R. K. (2021). Green synthesis of nanoparticles using plant extracts: A review. *Environmental Chemistry Letters*, 19(1), 355-374. doi.org/10.1007/s10311-020-

01074-x.

19. Shanker, U., Jassal, V., Rani, M., & Kaith, B. S. (2016). Towards green synthesis of nanoparticles: from bio-assisted sources to benign solvents. A review*. International Journal of Environmental Analytical Chemistry*, 96(9), 801-835. doi: 10.1080/03067319.2016.1209663.
20. Bharathi, D., Kalaichelvan, P. T., Atmaram, V., & Anbu, S. (2016). Biogenic synthesis of silver nanoparticles from aqueous flower extract of Bougainvillea spectabilis and their antibacterial activity. *J. Med. Plants*, 4(5), 248-252. ISSN 2320-3862.
21. Moodley, J. S., Krishna, S. B. N., Pillay, K., & Govender, P. (2018). Green synthesis of silver nanoparticles from Moringa oleifera leaf extracts and its antimicrobial potential. *Advances in Natural Sciences: Nanoscience and Nanotechnology*, 9(1), 015011. doi.10.1088/2043-6254/aaabb2
22. Nevárez-Martínez, M. C., Kobylański, M. P., Mazierski, P., Wółkiewicz, J., Trykowski, G., Malankowska, A., ... & Zaleska-Medynska, A. (2017). Self-organized TiO_2–MnO_2 nanotube arrays for efficient photocatalytic degradation of toluene. *Molecules*, 22(4), 564. doi.org/10.3390/molecules22040564.
23. Alonso, D. M., Wettstein, S. G., & Dumesic, J. A. (2012). Bimetallic catalysts for upgrading of biomass to fuels and chemicals. *Chemical Society Reviews*, *41*(24), 8075-8098. doi.org/10.1039/C2CS35188A.
24. López-Mercado, J., Nambo, A., Toribio-Nava, M. E., Melgoza-Sevilla, O., Cázarez-Barragán, L., Cajero-Zul, L., ... & Cardenas-Galindo, M. G. (2018). High and low esterification degree pectins decomposition by hydrolysis and modified Maillard reactions for furfural production. *Clean Technologies and Environmental Policy*, 20(7), 1413-1422. doi.org/10.1007/s10098-018-1570-y.
25. Guízar-Amezcua, M. G., Pineda-Santana, A., González-Domínguez, M. I., Cajero-Zul, L. R., Guerrero-Ramírez, L. G., López-Miranda, A., ... & López-Mercado, J. (2022). Evaluation of pectin extractions and their application in the alkaline Maillard reaction. Scientific Reports, 12(1), 1-12. doi.org/10.1038/s41598-022-22002-9.
26. Valderrama-Bravo, C., Gutiérrez-Cortez, E., Contreras-Padilla, M., Oaxaca-Luna, A., Del Real López, A., Espinosa-Arbelaez, D. G., & Rodríguez-García, M. E. (2013). Physico-mechanic treatment of nixtamalization by-product (nejayote). *CyTA-Journal of Food*, 11(sup1), 75-83. doi.org/10.1080/19476337.2013.781680.
27. Goutam, S. P., Saxena, G., Singh, V., Yadav, A. K., Bharagava, R. N., & Thapa, K. B. (2018). Green synthesis of TiO2 nanoparticles using leaf extract of Jatropha curcas L. for photocatalytic degradation of tannery wastewater. Chemical Engineering Journal, 336, 386-396. doi.org/10.1016/j.cej.2017.12.029.
28. Vimalkumar, C. S., Hosagaudar, V. B., Suja, S. R., Vilash, V., Krishnakumar, N. M., & Latha, P. G. (2014). Comparative preliminary phytochemical analysis of ethanolic extracts of leaves of Olea dioica Roxb., infected with the rust fungus Zaghouania oleae (EJ Butler) Cummins and non-infected plants. *Journal of Pharmacognosy and phytochemistry*, 3(4). E-ISSN: 2278-4136.
29. Mahesh A.R., Ranganath M.K. and Harish Kumar D.R. (2013). Enrichment of Flavonoids from the Methanolic Extract of Boerhaavia Diffusa Roots by Partitioning Technique. *Research Journal of*

Chemical Sciences. Vol. 3, pp: 43-47. ISSN 2231-606X.

30. Tamilselvan A., Srividhya P., Karuthapandian S. and Mehalingam P. (2016). Plant - Driven to Synthesis of Silver Nanoparticles using Crataeva religiosa Hook & Frost and its Utility in Detecting Antimicrobial and Antioxidant Assay. *International Journal of Green and Herbal Chemistry.* Vol. 5, pp: 390-402.
31. Aslam, M., Abdullah, A. Z., & Rafatullah, M. (2021). Recent development in the green synthesis of titanium dioxide nanoparticles using plant-based biomolecules for environmental and antimicrobial applications. Journal of Industrial and Engineering Chemistry, 98, 1-16. doi.org/10.1016/j.jiec.2021.04.010
32. Mintiwab, A., & Jeyaramraja, P. R. (2021). Evaluation of phytochemical components, antioxidant and antibacterial activities of silver nanoparticles synthesized using Ricinus communis leaf extracts. *Vegetos*, 34(3), 606-618. doi.org/10.1007/s42535-021-00244-8.
33. Pushpamalini, T., Keerthana, M., Sangavi, R., Nagaraj, A., & Kamaraj, P. (2021). Comparative analysis of green synthesis of TiO2 nanoparticles using four different leaf extract. Materials Today: Proceedings, 40, S180-S184. doi.org/10.1016/j.matpr.2020.08.438.
34. Sundrarajan, M., & Gowri, S. (2011). Green synthesis of titanium dioxide nanoparticles by Nyctanthes arbor-tristis leaves extract. *Chalcogenide Lett*, *8*(8), 447-451.
35. Shimi, A. K., Ahmed, H. M., Wahab, M., Katheria, S., Wabaidur, S. M., Eldesoky, G. E., ... & Rane, K. P. (2022). Synthesis and applications of green synthesized TiO2 nanoparticles for photocatalytic dye degradation and antibacterial activity. *Journal of Nanomaterials*, *2022*. doi.org/10.1155/2022/7060388.
36. Madadi, Z., & Bagheri Lotfabad, T. (2016). Aqueous extract of acanthophyllum laxiusculum roots as a renewable resource for green synthesis of nano-sized titanium dioxide using sol-gel method. *Advanced Ceramics Progress*, *2*(1), 26-31. doi.10.30501/ACP.2016.70015.
37. Logeswari, P., Silambarasan, S., & Abraham, J. (2013). Ecofriendly synthesis of silver nanoparticles from commercially available plant powders and their antibacterial properties. *Scientia Iranica*, *20*(3), 1049-1054. doi.org/10.1016/j.scient.2013.05.016.
38. Crist, B. V. Handbook of Monochromatic XPS Spectra Polymers and Polymers Damaged by X-rays.
39. Muniandy, S. S., Kaus, N. H. M., Jiang, Z. T., Altarawneh, M., & Lee, H. L. (2017). Green synthesis of mesoporous anatase TiO_2 nanoparticles and their photocatalytic activities. *RSC advances*, 7(76), 48083-48094. doi.org/10.1039/C7RA08187A
40. Atchudan, R., Edison, T. N. J. I., Perumal, S., Vinodh, R., & Lee, Y. R. (2018). In-situ green synthesis of nitrogen-doped carbon dots for bioimaging and TiO_2 nanoparticles@ nitrogen-doped carbon composite for photocatalytic degradation of organic pollutants. *Journal of Alloys and Compounds*, *766*, 12-24. doi.org/10.1016/j.jallcom.2018.06.272Get rights and content
41. Santhi, S. characterization of TiO_2 nanorods by hydrothermal method with different pH conditions and their photocatalytic activity. Appl. Surf. Sci, (500). doi.org/10.1016/j.apsusc.2019.144058.

42. Ouerghi, O., Geesi, M. H., Riadi, Y., & Ibnouf, E. O. (2022). Limon-citrus extract as a capping/reducing agent for the synthesis of titanium dioxide nanoparticles: characterization and antibacterial activity. *Green Chemistry Letters and Reviews*, *15*(3), 483-490. doi.org/10.1080/17518253.2022.2094205.
43. Hariharan, D., Christy, A. J., Mayandi, J., & Nehru, L. C. (2018). Visible light active photocatalyst: Hydrothermal green synthesized TiO2 NPs for degradation of picric acid. *Materials Letters*, *222*, 45-49. doi.org/10.1016/j.matlet.2018.03.109.
44. Acosta, B., Smolentseva, E., Beloshapkin, S., Rangel, R., Estrada, M., Fuentes, S., & Simakov, A. (2012). Gold supported on ceria nanoparticles and nanotubes. *Applied Catalysis A: General*, 449, 96-104. doi.org/10.1016/j.apcata.2012.09.045.
45. Hafez, H., Wu, J., Lan, Z., Li, Q., Xie, G., Lin, J., ... & Abdel-Mottaleb, M. S. (2010). Enhancing the photoelectrical performance of dye-sensitized solar cells using TiO2: Eu3+ nanorods. *Nanotechnology*, *21*(41), 415201. doi 10.1088/0957-4484/21/41/415201.
46. Alonso, D. M., Wettstein, S. G., Mellmer, M. A., Gurbuz, E. I., & Dumesic, J. A. (2013). Integrated conversion of hemicellulose and cellulose from lignocellulosic biomass. *Energy & Environmental Science*, *6*(1), 76-80. doi 10.1039/C2EE23617F.
47. Gallo, J. M. R., Alonso, D. M., Mellmer, M. A., Yeap, J. H., Wong, H. C., & Dumesic, J. A. (2013). Production of furfural from lignocellulosic biomass using beta zeolite and biomass-derived solvent. *Topics in Catalysis*, *56*, 1775-1781. doi.org/10.1007/s11244-013-0113-3.
48. Mellmer, M. A., Sener, C., Gallo, J. M. R., Luterbacher, J. S., Alonso, D. M., & Dumesic, J. A. (2014). Solvent effects in acid-catalyzed biomass conversion reactions. *Angewandte chemie international edition*, *53*(44), 11872-11875. doi.org/10.1002/anie.201408359.

Figures

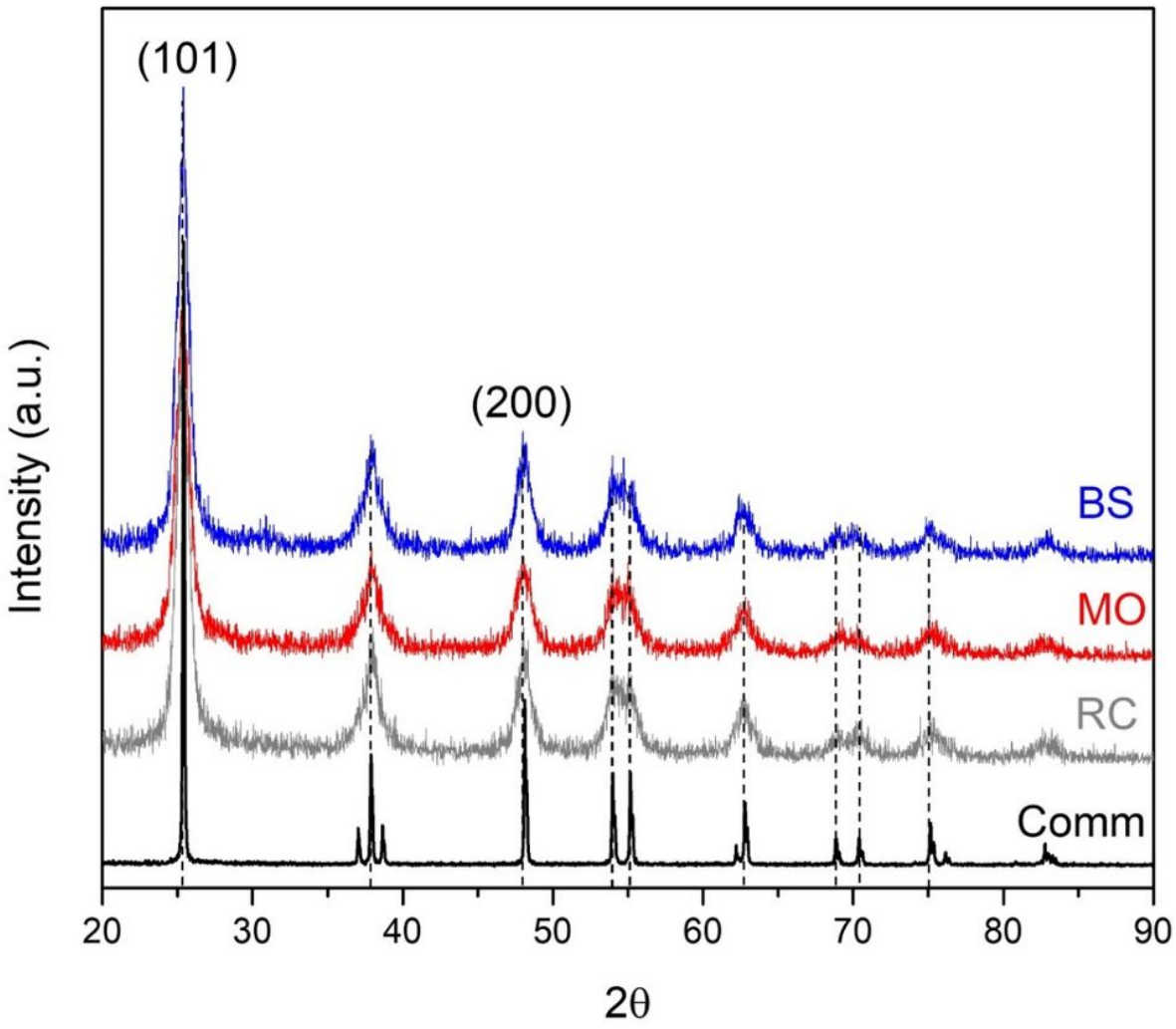

Figure 1

X-ray diffraction patterns of TiO_2 samples prepared under a green synthesis from different plant extracts: *Ricinus communis* (RC), *Moringa oleífera* (MO) and *Bougainvillea spectabilis* (BS). A diffractogram from commercial TiO_2 (Comm) is presented as a reference. Bragg index corresponds to the PDF 00-064-0863 chart.

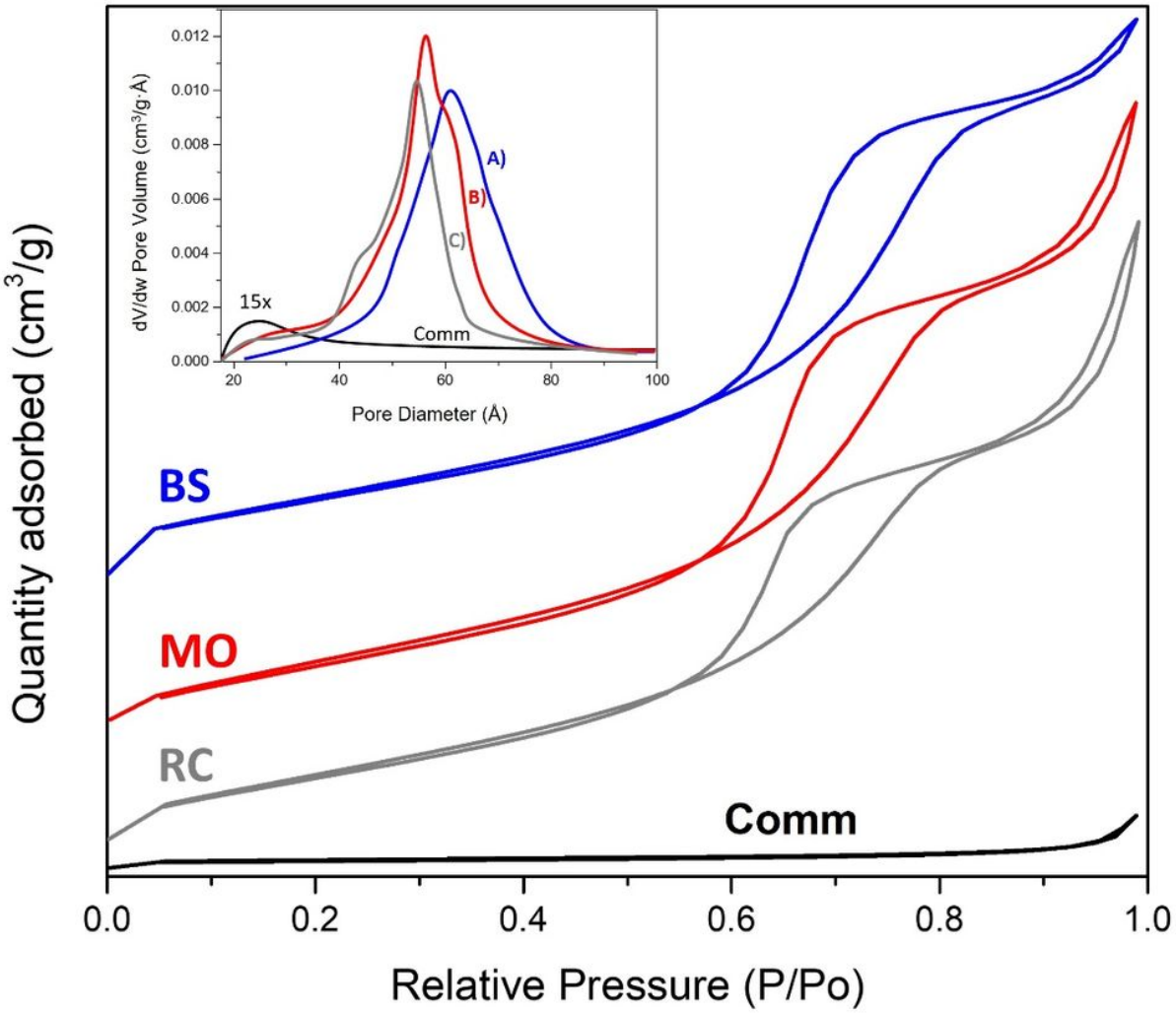

Figure 2

Isotherms of N_2 adsorption for the greenly synthesized TiO_2 samples using plant extracts of BS, MO and RC and comm TiO_2 as a reference sample. The inset presents the corresponding pore size distribution.

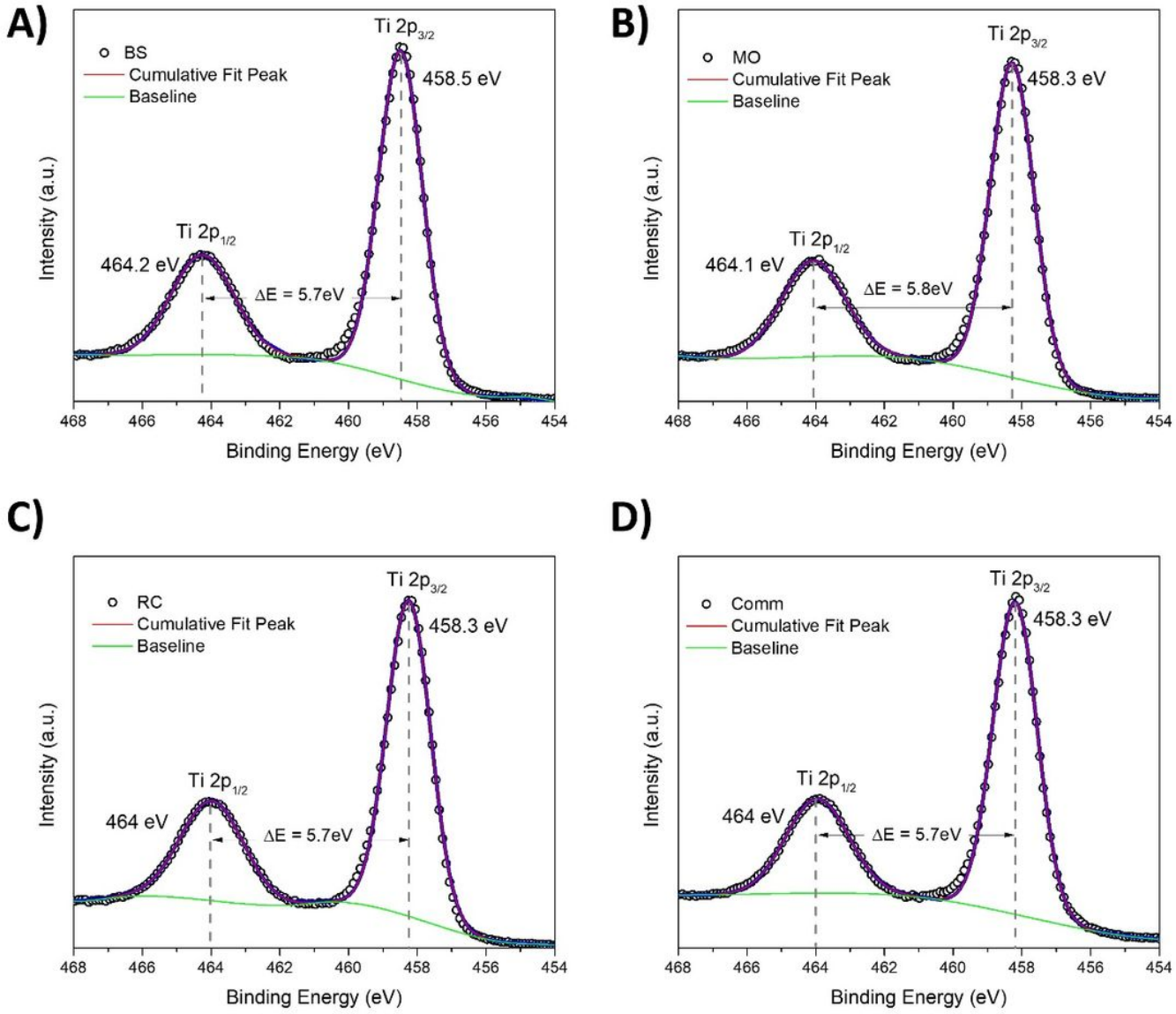

Figure 3

Ti2p XP spectra for the TiO_2 samples prepared with the plant extract BS (A), MO (B) and RC (D) and the reference comm TiO_2 (D). The circles represent the experimental data; the blue curves represent the Gaussian fits of the experimental data.

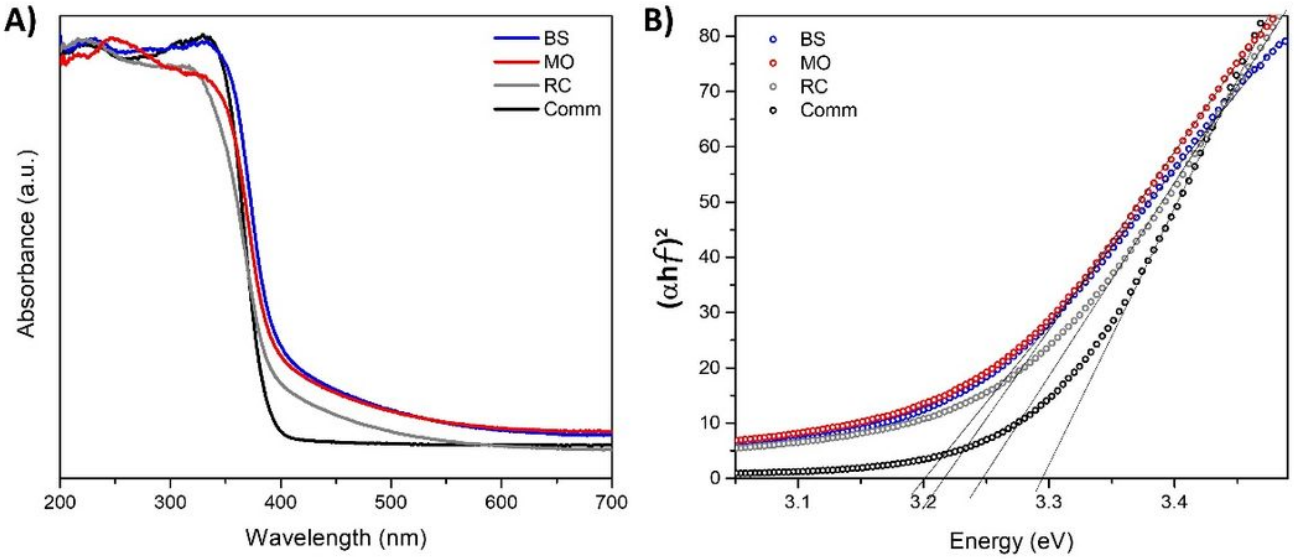

Figure 4

A) UV-Vis absorption spectra of TiO_2 samples prepared via green synthesis using extracts of BS, MO and RC. The UV-Vis spectrum of commercial TiO_2 (Comm) is presented as a reference. B) Estimation of band gap energies based on the Tauc plot method.

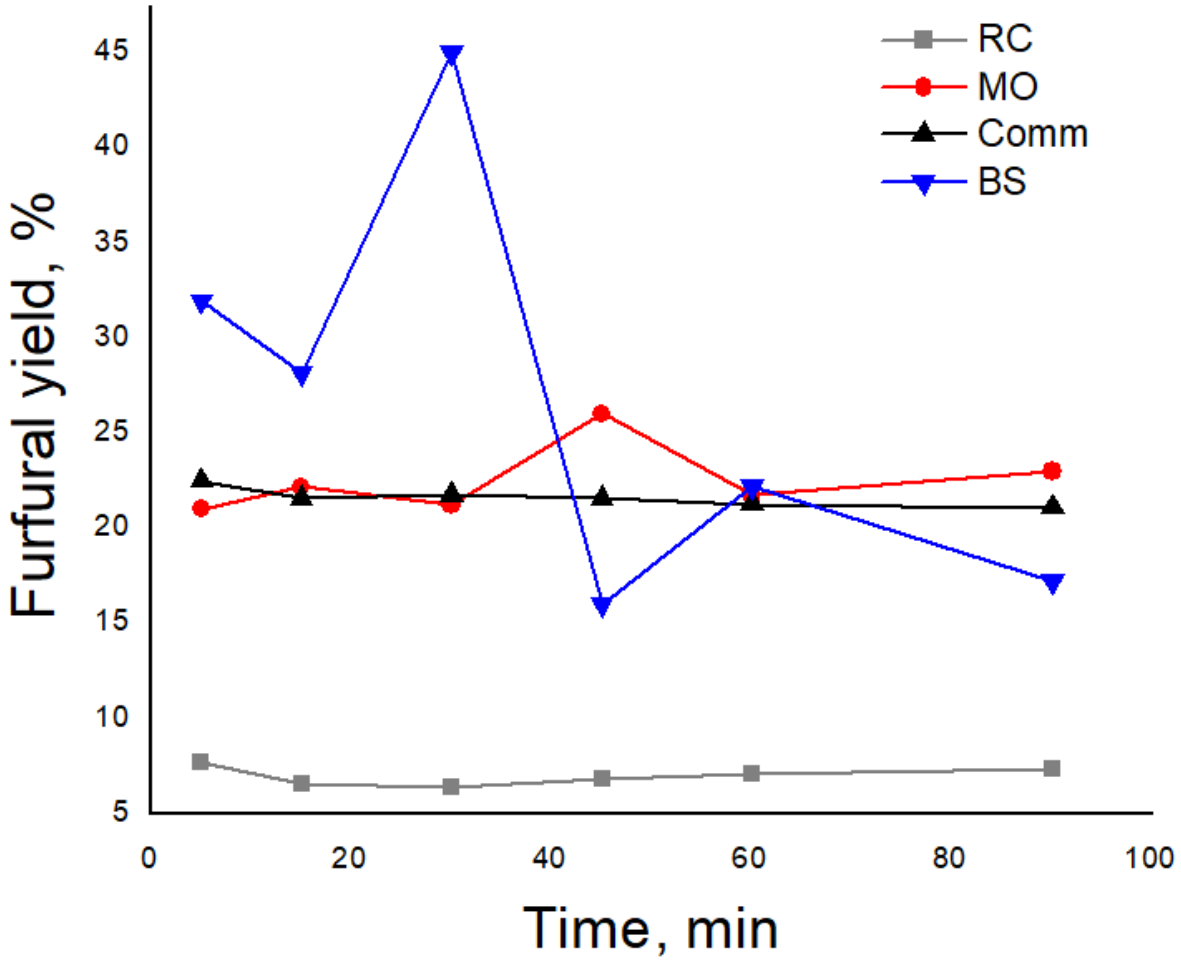

Figure 5

Furfural yield versus time from nejayote conversion using TiO_2 comm and TiO_2 sample prepared via green synthesis using extracts of BS, MO and RC at room temperature.

Supplementary Files

This is a list of supplementary files associated with this preprint. Click to download.

- FiguresandtablesS.docx